Materials Research Proceedings 41 (2024) 1668-1677 https://doi.org/10.21741/9781644903131-185

Numerical investigation of rotational friction welding for C22.8 - 41Cr4 joints using a substitute model

MOHNFELD Norman[1,a*], WESTER Hendrik[1], TUNC KARAER Gökhan[1], PIWEK Armin[1] and UHE Johanna[1,b]

[1]Institute of Forming Technology and Machines (LUH), An der Universität 2, 30823 Garbsen, Germany

[a]mohnfeld@ifum.uni-hannover.de, [b]uhe@ifum.uni-hannover.de

Keywords: Rotational Friction Welding, FEM, Hybrid Components, Substitute Model

Abstract. Rotational friction welding (RFW) is a solid-state joining process that enables the joining of similar and dissimilar materials such as metal-metal or metal-ceramic joints. Due to its high application flexibility, this process has great potential for the production of hybrid components. In order to be able to realise this potential for the production of hybrid components, the development of an improved process design is required. Due to the complexity of the process, the Finite Element Method (FEM) can be used to solve complex problems and is therefore an established tool for the design of joining processes. This work focuses on the development of an FE model to represent the RFW process of C22.8 and 41Cr4 joints. The material data required for the numerical representation of the RFW were obtained from isothermal cylinder compression tests. The frictional heat which is generated during RFW is calculated using a substitute model, which mainly depends on the Y-factor. The Y-factor indicates what percentage of the calculated frictional energy is introduced into the process. The Y-factor was determined and then verified using experimental data. A general validity of the determined Y-factors with changed process parameters could not be achieved.

Introduction

Rotational friction welding (RFW) as a solid-state joining process represents a promising process for the economic production of hybrid high-performance components. Compared to conventional fusion-metallurgical welding processes, the RFW is characterised by short welding times, high geometrical accuracy, low energy consumption, excellent static and dynamic bond strengths with fine grain structure and large material variety [1]. Furthermore, RFW can be used to join materials that can only be welded to a limited extent or not at all using conventional fusion welding processes (e.g. aluminium-copper or steel-ceramic) [2]. The design of RFW processes is complicated due to the rapid process dynamics and the complexity of the material phenomena involved. With regard to the methodical design and development of production processes, the finite element method (FEM) is a proven instrument for tool and process design of bulk metal forming as well as joining processes. Time-consuming and cost-intensive steps in the product development phase can be reduced and the existing process limits can be systematically expanded through virtual testing of new materials or process variants [3]. Soucail et al. investigated a thermo-mechanically coupled FE simulation of friction welding process using the lagrangian formulation with an explicit scheme. A good agreement with the experimentally measured temperature profiles near the weld seam could be achieved. At a distance of 0.3 mm, however, the calculation results deviated considerably from the experimental measurements [4]. A cooling simulation decoupled from the friction welding process was carried out by Nguyn et al.. Cooling curves were taken from the experiment and applied to the workpieces. Using microstructure models and experimental time-temperature-conversion diagrams, an estimation of the phase fractions after cooling could be made, whereby the workpieces were modelled in the FE simulation as rigid bodies without plastic

deformation [5]. Schmicker conducted a simulation study of the friction welding of a mono material steel joint. Using fluid-dynamic material models, a high reproduction quality of the plastic material flow could be achieved in a MATLAB environment. However, due to the lack of structural-mechanical coupling, the elastic strains and thermal shrinkage were not taken into account [6]. Nu et al. numerically investigated a friction welded joint made of a Ti-alloy. The frictional heat was simplified as a constant heat flux density, which was interrupted when the melting temperature was reached. Although experimental investigations were presented in the paper, no comparison was made with the numerical results [7]. A welded joint made of a Ni alloy was also modelled by Wang et al. using ABAQUS. In the process parameter study, the influence of the rotational speed on the resulting part shortening and the temperature development was investigated without an experimental validation of the results [8]. In a study by Li et al. the temperature development at the beginning of the process was modelled with analytical approaches. Validation was based on a peak temperature measurement using a thermographic camera [9]. Friction welding processes for a Ni-alloy and a CrNi stainless steel were modelled with DEFORM by Nan et al.. In principle, a good temperature prediction could be achieved, considering only a locally undefined peak temperature at the surface. From the comparison of the weld flash geometry, it could be deduced that the component geometry was underestimated by the FE model [10].

In summary, either the temperature development was considered without including the plastic deformation or the forming was simulated and the heating was modelled by an external heat source.

Using RFW, similar and dissimilar joints can be produced that have sufficient strength for subsequent forming. RFW is therefore a promising approach for the production of hybrid components. In the Collaborative Research Centre (CRC) 1153 Tailored Forming, hybrid semi-finished products consisting of different steels or steel and aluminium are produced using RFW [11]. The design of the RFW processes as well as the investigation of the influence of the specimen geometries on the composite strengths was determined by experimental tests in previous studies of the authors [12,13]. By a numerical consideration of the RFW process, extensive experimental investigations can be reduced on the one hand and on the other hand the analyses in the joining zone can be carried out without destroying the component. Furthermore, it is possible to integrate subroutines into the model so that, for example, the microstructure transformation processes or the bond strength can be represented.

This work deals with the numerical representation of the RFW process of C22.8 and 41Cr4. In order to describe the thermomechanical material behaviour during friction welding, process flow properties are determined by means of isothermal cylinder compression tests in a temperature range from 20 °C to 1,400 °C. Based on the results analytical material models are created and implemented in the FE-software using subroutines. The RFW process is setup as a 2D model in the commercial FE software Simufact.forming v16 (simufact engineering GmbH, Hamburg, Germany). First, the influence of the mesh size on the results is analysed. Subsequently, the Y-factor of the substitute model for calculating the frictional heat in the process is examined and investigated. Finally, the simulation model is verified using the inversely determined Y-factors and finally validated by varying the various process parameters.

Methods - Experimental Investigation

Experimental Investigation: To determine the chemical composition of the materials used, measurements were carried out on the SPECTROMAXx radio spectrometer in argon atmosphere. Each material was radioed nine times for statistical validation of the measurement. The results of the radio spectroscopy measurement of the investigated materials are listed in Table 1. It is noticeable that for both materials a carbon value slightly below the prescribed minimum value was measured. In addition, 41Cr4 has a slightly higher chromium content. All other measured values are within the specified tolerance ranges.

Table 1. Chemical composition of the C22.8 and 41Cr4 steels in wt.%., measured by optical emission spectrometry.

Element		C	Si	Mn	P	S	Cr	Mo	Ni	Al	Co	Cu
C22.8	Max	0.23	0.4	0.9	0.025	0.015	0.3	0.1	0.3	0.05	0.1	0.4
	Min	0.18	-	0.3	-	-	-	-	-	0.015	-	-
	Test	**0.166**	**0.208**	**0.817**	**0.005**	**0.005**	**0.116**	**0.022**	**0.095**	**0.023**	**0.008**	**0.196**
41Cr4	Max	0.45	0.4	0.9	0.035	0.03	1.2	0.1	0.3	-	0.1	0.4
	Min	0.38	-	0.6	-	-	0.9	-	-	-	-	-
	Test	**0.36**	**0.305**	**0.795**	**0.004**	**0.017**	**1.24**	**0.01**	**0.024**	**0.001**	**0.001**	**0.013**

To describe the flow behaviour cylinder compression tests were carried out for C22.8 and 41Cr4 according to the parameters listed in Table 2.

Table 2. Experimental parameters for the cylinder compression tests of C22.8 and 41Cr4.

material	strain rate in s^{-1}	temperature in °C
C22.8	0.1; 1; 10	1,300 and 1,400
41Cr4	0.1; 1; 10	1,300 and 1,400

The specimen geometry was Ø 10 mm x 15 mm and specimens were prepared from plane-parallel discs by wire erosion. The compression tests were carried out on the Gleeble 3800 GTC forming simulator. Under vacuum, the specimens were heated conductively at a heating rate of 4.5 K/s and held at the target temperature for 30 s to realise a homogeneous temperature distribution. Since partially liquid phases are already formed at this temperature, the specimens are compressed in a quartz sleeve. The quartz sleeve shields the specimen so that no particles can damage the test chamber. The punches are made of solid hard metal, which has a very high heat resistance. For the strain rates of 1 s^{-1} and 10 s^{-1} the tests were displacement controlled and for 0.1 s^{-1} strain controlled. The specimens were upset to a plastic strain of 0.7. Each parameter combination from Table 2 was repeated five times. For the temperature range below 1,300 °C up to room temperature, flow curves were also recorded from the same material batch by cylinder compression tests [14].

The experimental investigations of the RFW process were carried out on the Genius Plus RS30 from KUKA. On the spindle side, a cylinder made of 41Cr4 with a Ø 40 mm and a length of 160 mm was inserted. A cylinder made of C22.8 with a Ø 40 mm and a length of 210 mm was used on the sledge side. The temperature measurement was carried out with a type S thermocouple. According to Fig. 1 (a), eight type K thermocouples (TC) were attached to the C22.8 bolts. In order to measure the temperature in the contact surface of the friction partners TC1 and TC5 were guided directly into the end face via small grooves. At 90° to this, measurements were taken axially around the circumference at a distance of 5 mm, 10 mm and 15 mm from the end face (TC2-TC4 and TC6-TC8). This allows the heat dissipation along the specimen to be determined. In addition, force, displacement as well as the rotational speed are recorded during the experiments. The applied time-rotational speed and force-time profiles for the 1 parameter set and 2 parameter set is shown in Fig. 1 (b). In the friction phase, heat is generated by the rotation and the applied axial force. By stopping the spindle, the upsetting phase is initiated and the bond is created. Fig. 1 (a) shows the process at the beginning of the friction phase on the left and after the end of the upsetting phase on the right. The RFW tests were repeated five times using this 1 parameter set with a rotational speed of 1,500 min^{-1} and a upsetting force of 180 kN. In addition, a test with increased rotational speed of 2,000 min^{-1} and increased upsetting force of 220 kN was carried out for later model validation in 2 parameter set. One specimen was shortened and separated along the

longitudinal axis by wire erosion and prepared metallographically and measured with the Keyence VR-3200 Profilometer. By etching with 5 % nitric acid (HNO3), the structural changes in the friction welding zone was analysed.

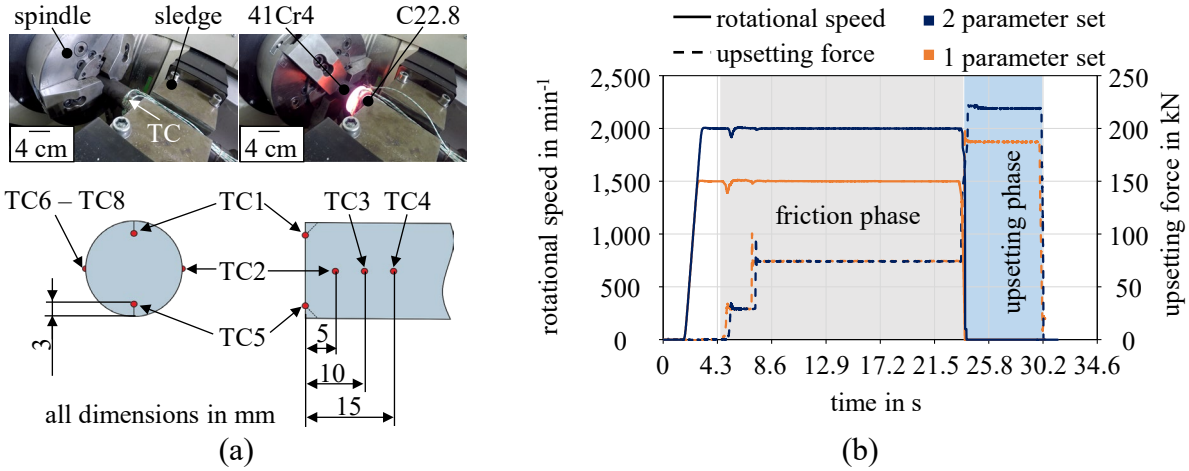

Fig. 1 (a) RFW process at the beginning of the friction phase and at the end of the upsetting phase as well as the schematic positioning of the thermocouples; (b) rotational speed and upsetting force time curve for the 1 parameter set and 2 parameter set experiments.

Numerical Investigation

The RFW process was setup as a 2D model in the simulation software Simufact.forming v16. For this purpose, two cylinders were created as workpieces according to the dimensions of the experiments and axially aligned, see Fig. 2. The modified material models were assigned to the two workpieces according to the experimental arrangement. Upper, lower and support dies were defined as rigid bodies. A spring force was applied between the support die and the upper die to apply the upsetting force. The course of the spring force was determined from the experiments and assigned to the spring. The positions of both the support die and the lower die are stationary in the room in order to feed the spring force into the welding zone. The upper die is movable in z-direction. Particles have been attached to the welding zone on the C22.8 workpiece, with the same spacing as the thermocouples in the experiments, compare Fig. 1 (a), which allow the temperature to be tracked through the process. The friction model according to Tresca with a friction factor of m = 0.3 was used to model the contact between the two workpieces. To analyse the geometry of the weld flash, a subroutine was used which records outer contour of the workpieces within a text file from the last increment. In this way, the influence of the model parameters on the weld flash formation can be precisely observed and compared. The friction welding module of Simufact.forming allows the use of a 2D process, as the rotational movement and the resulting frictional heat are calculated via a substitute model. This significantly reduces the simulation time and simplifies the kinematic mapping of the process.

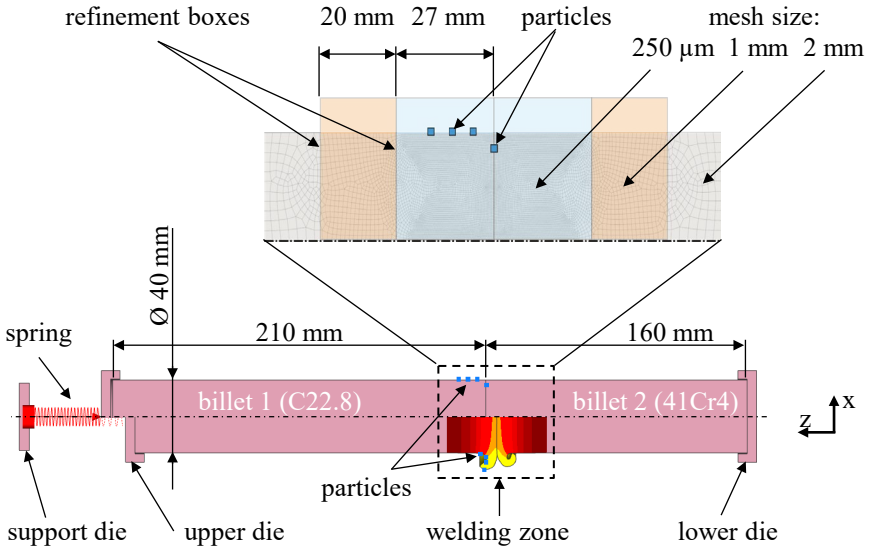

Fig. 2 Configuration of the FE model and position of the refinement boxes.

The frictional heat calculated by the equivalent model depends on the normal force, the rotational speed and the Y-factor. The Y-factor may range from 0.0 to 1.0 and indicates what percentage of the calculated frictional energy is introduced into the process [15]. The Y-factors can be specified depending on the temperature. In this way, for example, a change of frictional heat generation near the melting point can be taken into account. Due to the doughy/liquid state, no further frictional energy is generated in the real process until the temperature drops again below the melting point of approximately 1,490 °C. This can be realised by a Y-factor of 0.0 at the melting temperature of the material. Zhang et al. used Simufact.forming for a friction stir rivet welding process and stated that they had used a temperature-dependent Y-factor for AA6061-T6 sheet [16]. Kubit and Trzepiecinski also use the friction welding module of Simufact.forming to model friction stir spot welding Alclad 7075-T6 aluminium alloy sheets. They stated that they use a temperature-dependent Y-factor [17]. In this work, the Y-factor was also modeled as a function of temperature, see Table 3. The Y-factors were determined iteratively by comparing numerically determined and experimentally measured temperature curves. The resulting temperature curves were compared with the experimental curves of the 1 parameter set, allowing the appropriate Y-factors to be determined.

Table 3. Values of the examined Y-factors.

Y-factor	0.7	0.7	0.5	0.45	0.233	0.0
temperature	20 °C	300 °C	600 °C	1,200 °C	1,400 °C	1,490 °C

The workpieces are meshed with elements of the type Quads (10). To ensure that the results are independent of the selected element size, the element size was varied from 6 mm to 0.25 mm. The required calculation time increases exponentially with decreasing element size from 2 mm and reaches its maximum value of almost 350 min with an element size of 0.25 mm, see Fig. 3 (a).

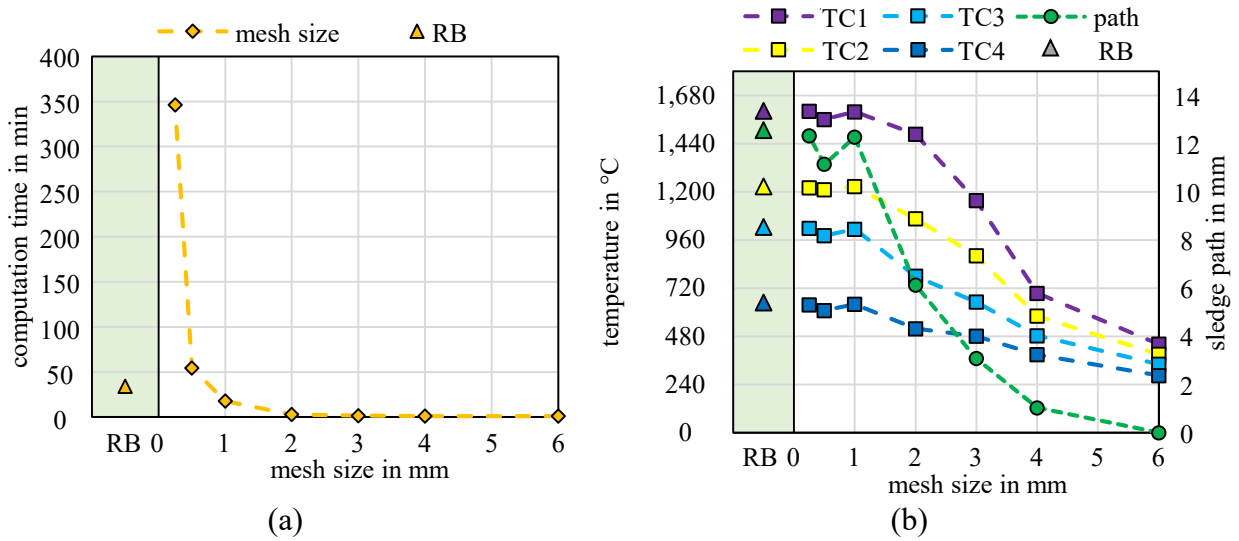

Fig. 3 Results of the mesh study: (a) computation time over mesh size; (b) development of the maximum temperatures and the sledge path over the mesh size.

The calculated maximum temperatures at the particles TC1-TC4 (squares) increase continuously until they stagnate at an element size of 1 mm and show convergence, Fig. 3 (b). The development of the maximum slide path (circle) over the element size is similar. Due to the comparatively long workpieces and the very localised deformation near the joining zone refinement boxes (RB, triangle) where used see Fig. 2. The workpiece was meshed with 2 mm element size and refined to 1 mm and 0.25 mm using two RB, coupled to the movements of the workpieces. By using the RB, the required calculation time can be reduced from 350 min to 35 min see Fig. 3 (a) and (b), thus saving resources.

Results and Discussion

The recorded flow properties at 1,300 °C and 1,400 °C are shown in Fig. 4. Both materials show similar flow characteristics. The flow stress decreases with increasing temperature, whereas the flow stress increases with increasing strain rate. In the temperature range investigated, the flow stress for the C22.8 is slightly higher than the flow stress of the 41Cr4. With the determined flow curves, the existing material models were extended so that the flow behaviour for C22.8 and 41Cr4 from 20 °C to 1,400 °C can now be de-scribed and used in the FE simulation.

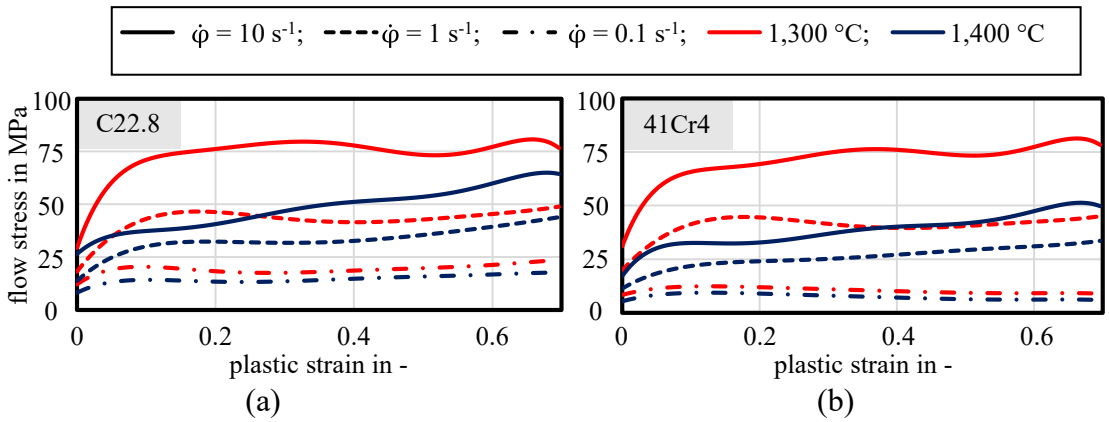

Fig. 4. Flow curves for (a) C22.8 and (b) 41Cr4 at 1,300 °C and 1,400 °C.

The Y-factor-temperature curve was fitted in such a way that the best possible agreement could be achieved with the experimentally recorded temperature curves, sledge path and weld flash geometry of the 1 parameter set. In Fig. 5 (a)-(d) the experimental temperature curves of the

respective thermocouples are compared to the simulated curves. The temperature curves of the axially attached particles lie within the scatter range of the experimental curves (Fig. 6 (b)-(d)). For TC1 and TC5, the experimental curves scatter very strongly. The reason for this is the high mechanical load in the front surface during the RFW process, which influences the results of the temperature measurement. Therefore, the temperature for TC1/TC5 is higher in the simulation, but remains below the melting temperature of 1,492 °C. A comparison of the simulated and experimental sledge path shows no deviations during the friction phase. The duration of the upsetting phase as well as the steep increase of the sledge path is also well predicted with the FE model Fig. 6 (e). However, the maximum sledge path is underestimated by approx. 2 mm in the simulation. In addition, the simulated sledge path runs constant after reaching the maximum, while in the experiment the sledge path continues to increase. Possible reasons for the deviations could be due to the machine stiffness or to slipping of the specimen in the clamping jaws of the sledge. These effects are not taken into account in the simulation. In Fig. 6 (f), a friction welded specimen is shown in longitudinal section, with the simulated contours superimposed. The specimen was etched so that the joining zone and the heat-affected zone are visible. With the simulated flash geometries, the flash geometries of the experiments were well predicted. Only in the case of 41Cr4 slight deviations in the radii and in the transition from the initial diameter to the weld flash are visible. Apart from the deviation at TC1 and the maximum sledge path, a successful model verification was achieved, which predicts the experimental results well.

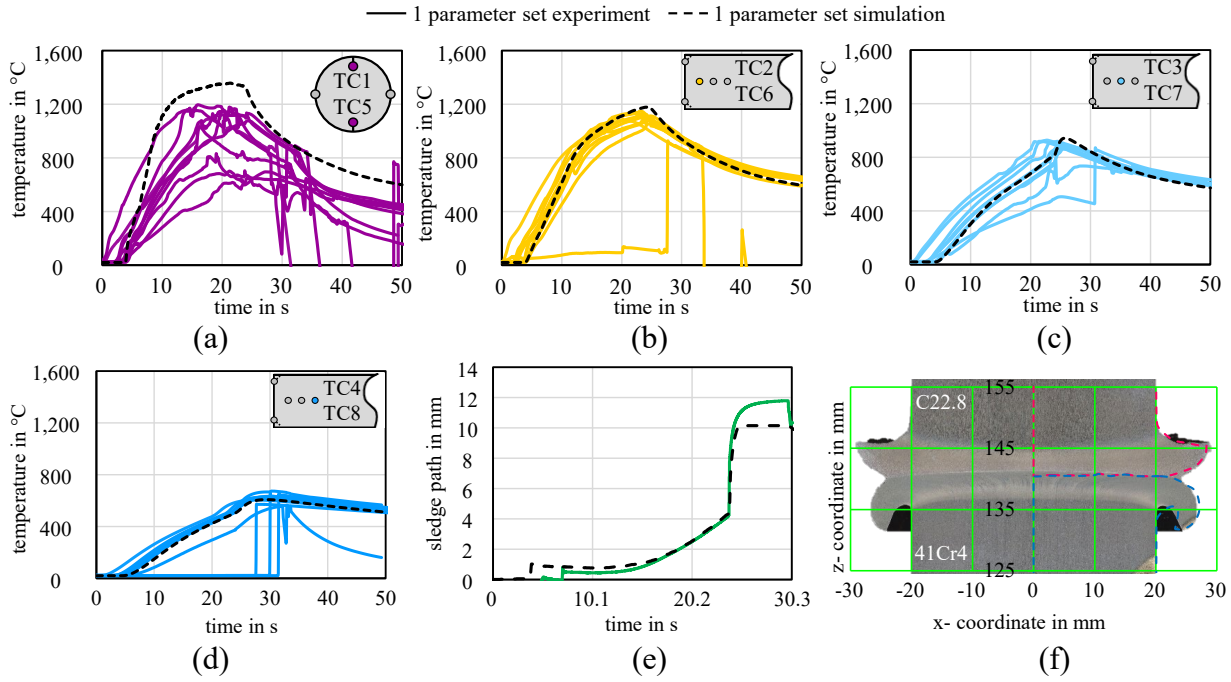

Fig. 5 Comparison of the 1 parameter set of the experimental and simulated results [18] (a) temperature-time curves of TC1 and TC5; (b) temperature-time curves of TC2 and TC6; (c) temperature-time curves of TC3 and TC7; (d) temperature-time curves of TC4 and TC8; (e) Sledge path time curves; (f) weld flash geometry of C22.8 and 41Cr4.

Finally, a simulation with the 2 parameter set was carried out with the verified Y-factor-temperature curve in order to examine the general validity of the determined Y-temperature curve. During the 2 parameter set experiment, the rotational speed in the friction phase was increased to 2,000 min^{-1} and the upsetting force in the upsetting phase was increased to 220 kN, see Fig. 1 (b). Since the substitute model is not only based on the Y-factor but also on the rotational speed and the normal stress, it can be proofed whether the determined Y-factors also provide sufficiently

accurate results for varying process parameters. In Fig. 7 (a)-(d) the simulated and experimental temperature curves are compared. At all measuring points the simulation overestimates the temperature curves from the experiment. Especially in the friction phase, the temperature at TC1 rises steeply, resulting in a high amount of frictional heat in the contact zone, which is conducted into the workpiece. In the upsetting phase, on the other hand, cooling is well achieved. The increased temperature during the upsetting phase is due to the increased rotational speed, since the increase in upsetting force only takes effect in the upsetting phase. Due to the fact that too much frictional heat is calculated by the substitute model, the material already begins to flow during the friction phase, which leads to an overestimation of the sledge path in the friction phase, see Fig. 7 (e). As a result, the maximum sledge path of the simulation and the experiment are equal in the upsetting phase. Although the maximum sledge paths are identical, the simulated weld flash geometries clearly overestimate the real flash formation for both materials, see Fig. 7 (f). Due to the effects of machine stiffness or slipping of the workpiece, which are not shown, the maximum sledge path should not be used as the basis for evaluation, but rather the sledge path at the end of the friction phase. A successful validation of the determined Y-factors on changed process parameters is therefore not given. For this purpose, further investigations must be carried out on the influence of the rotational speed and the upsetting force in combination with the Y-factor during the friction phase.

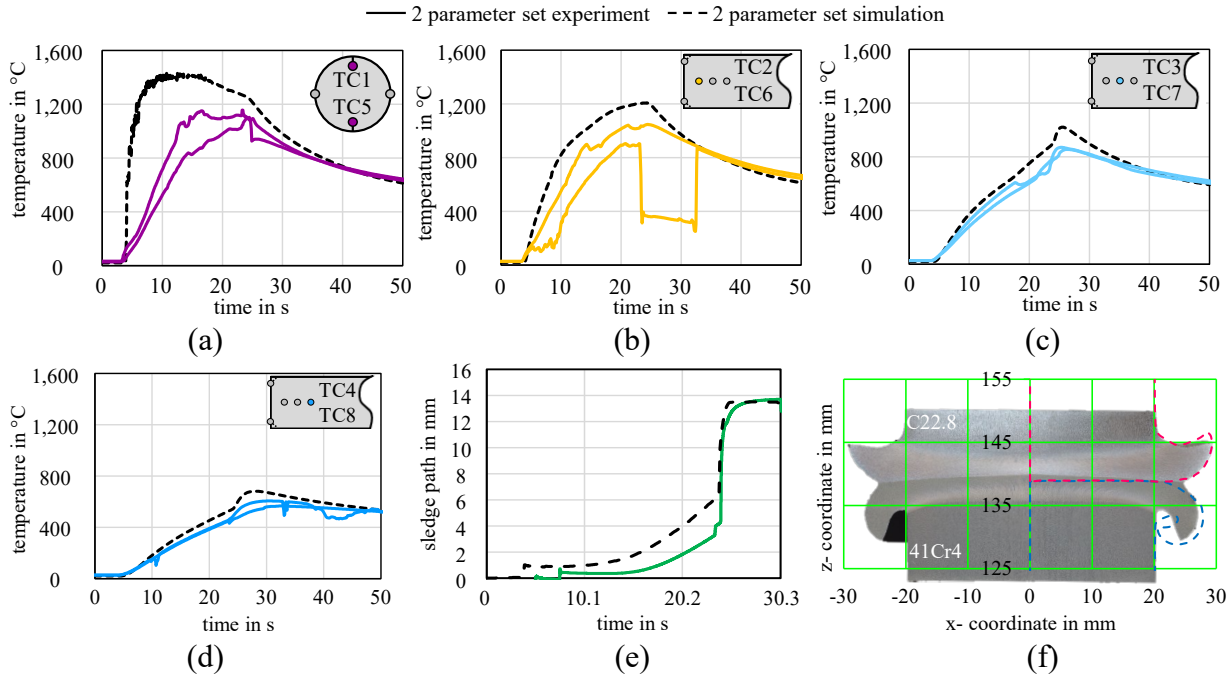

Fig. 6 Comparison of the 2 parameter set of the experimental and simulated results [19] (a) temperature-time curves of TC1 and TC5; (b) temperature-time curves of TC2 and TC6; (c) temperature-time curves of TC3 and TC7; (d) temperature-time curves of TC4 and TC8; (e) sledge path time curves; (f) weld flash geometry of C22.8 and 41Cr4.

Summary and Conclusions

In this article, the RFW process was modelled by means of FEM using Simufact.forming. The focus was on the calculation of the frictional heat via a substitute model which is dependent on the Y-factor, the rotational speed and the normal stress. First of all, the existing material models for C22.8 and 41Cr4 were extended for a temperature range up to 1,400 °C by means of cylinder compression tests. After the mesh study was carried out, the influence of the Y-factor on the temperature, the sledge path as well as the weld flash geometry was investigated. A Y-temperature curve was fitted to the results of the experiments of the 1 parameter set and verified. Finally, the

Y-temperature curve was tested regarding the validity for the process parameters of the 2 parameter set. From this work it can be concluded that the RFW can be reproduced with the substitute model in Simufact.forming. By fitting a Y-factor-temperature curve to the experimentally recorded data, it was possible to correctly predict the RFW numerically. However, this Y-factor-temperature curve is not generally valid, as the comparison with further experimental data has shown. Thus, it is possible to numerically predict the RFW correctly if the experimental data is available, but the model is currently not suitable for carrying out variations of process parameters.
Since the mathematical structure of the substitute model is not known, the exact mathematical relationships are unknown. Therefore, the frictional heat calculation should be determined by subroutines depending on the friction present and not via an substitute model where the exact physical relationships are unknown.

Acknowledgments
The results presented in this paper were obtained within the Collaborative Research Center 1153 “Process chain to produce hybrid high performance components by Tailored Forming” in the subproject A01 and B03, funded by the Deutsche Forschungsgemeinschaft (DFG, German Research Foundation)—252662854. The authors thank the German Research Foundation (DFG) for their financial support of this project.

References

[1] U. Dilthey, Schweißtechnische Fertigungsverfahren 2: Verhalten der Werkstoffe beim Schweißen; Springer-Verlag: Berlin/Heidelberg, 2005, ISBN 3-540-21674-X.

[2] T. Lienert, T. Siewert, S. Babu, V. Acoff, ASM handbook - Welding Fundamentals and Processes, 2nd print; ASM International: Metals Park, Ohio, 2015, ISBN 978-1-61503-133-7.

[3] W. Li, A. Vairis, M. Preuss, T. Ma, Linear and rotary friction welding review. International Materials Reviews 2016, 61, pp. 71–100. https://doi.org/10.1080/09506608.2015.1109214

[4] M. Soucail, A. Moal, L. Naze, E. Massoni, C. Levaillant, Y. Bienvenu, Microstructural Study and Numerical Simulation of Inertia Friction Welding of Astroloy. In Superalloys 1992 (Seventh International Symposium). Superalloys, 20–24 Sep. 1992; TMS, 1992 - 1992; pp. 847–856, ISBN 0-87339-189-6

[5] T.C. Nguyen, D.C. Weckman, A thermal and microstructure evolution model of direct-drive friction welding of plain carbon steel. Metall and Materi Trans B 2006, 37, pp. 275–292. https://doi.org/10.1007/BF02693157

[6] D. Schmicker, A holistic approach on the simulation of rotary friction welding; Berlin, 2015, ISBN 3737575177.

[7] H.T. My Nu, T.T. Le, L.P. Minh, N.H. Loc, A Study on Rotary Friction Welding of Titanium Alloy (Ti6Al4V). Advances in Materials Science and Engineering 2019, 2019, pp. 1–9. https://doi.org/10.1155/2019/4728213

[8] F.F. Wang, W.Y. Li, J.L. Li, A. Vairis, Process parameter analysis of inertia friction welding nickel-based superalloy. Int J Adv Manuf Technol 2014, 71, pp. 1909–1918. https://doi.org/10.1007/s00170-013-5569-6

[9] P. Li, J. Li, H. Dong, Analytical description of heat generation and temperature field during the initial stage of rotary friction welding. Journal of Manufacturing Processes 2017, 25, pp. 181–184. https://doi.org/10.1016/j.jmapro.2016.12.003

[10] X. Nan, J. Xiong, F. Jin, X. Li, Z. Liao, F. Zhang, J. Li, Modeling of rotary friction welding process based on maximum entropy production principle. Journal of Manufacturing Processes 2019, 37, pp. 21–27. https://doi.org/10.1016/j.jmapro.2018.11.016

[11] B.-A. Behrens, J. Uhe, Introduction to tailored forming. Prod. Eng. Res. Devel. 2021, 15, pp. 133–136. https://doi.org/10.1007/s11740-021-01022-w

[12] B.-A. Behrens, J. Uhe, T. Petersen, F. Nürnberger, C. Kahra, I. Ross, R. Laeger, Contact Geometry Modification of Friction-Welded Semi-Finished Products to Improve the Bonding of Hybrid Components. Metals 2021, 11. https://doi.org/10.3390/met11010115

[13] B.-A. Behrens, D. Duran, T. Matthias, I. Ross, Enhancement of the interface of friction welded steel-aluminium joints. Prod. Eng. Res. Devel. 2021, 15, pp. 169–176. https://doi.org/10.1007/s11740-020-00994-5

[14] B.-A. Behrens, A. Bouguecha, C. Bonk, T. Matthias, Importance of material and friction characterisation for FE-aided process design of hybrid bevel gears. In. Proceedings of the International Conference of Global Network for Innovative Technology and AWAM International Conference in Civil Engineering (IGNITE-AICCE'17): Sustainable Technology and Practice for Infrastructure and Community Resilience, Penang, Malaysia, 8–9 August 2017; pp. 190016.

[15] N. Schubert, A. Sterzig, R. Mauermann, S. Hilbers, P. Kolbe, C. Kuhn, Development of a Friction Welded Joint for Future Industrial Application. MSF 2019, 949, pp. 119–124. https://doi.org/10.4028/www.scientific.net/MSF.949.119

[16] P. Zhang, S. Zhao, W. Wang, H. Zhang, J. Zhang, C. Yang, Y. Wang, W. Wei, G. Ma, Numerical Simulation and Experimental Investigation of Friction Stir Rivet Welding Process for AA6061-T6. dtmse 2021. https://doi.org/10.12783/dtmse/ameme2020/35546

[17] A. Kubit, T. Trzepiecinski, A fully coupled thermo-mechanical numerical modelling of the refill friction stir spot welding process in Alclad 7075-T6 aluminium alloy sheets. Archiv.Civ.Mech.Eng 2020, 2020. https://doi.org/10.1007/s43452-020-00127-w

[18] N. Mohnfeld, Dataset: Temperature measurement Rotary friction welding 1setup. 2023, https://doi.org/10.25835/r2534sqw

[19] N. Mohnfeld, Dataset: Temperature measurement Rotary friction welding 2setup. 2024, https://doi.org/10.25835/2jc9g610